Modeling light scattered from and transmitted through dielectric periodic structures on a substrate

Wenbo Sun, Gorden Videen, Bing Lin, and Yongxiang Hu

Light scattering and transmission by rough surfaces are of considerable interest in a variety of applications including remote sensing and characterization of surfaces. In this work, the finite-difference time-domain technique is applied to calculate the scattered and transmitted electromagnetic fields of an infinite periodic rough surface. The elements of the Mueller matrix for scattered light are calculated by an integral of the near fields over a significant number of periods of the surface. The normalized Mueller matrix elements of the scattered light and the spatial distribution of the transmitted flux for a monolayer of micrometer-sized dielectric spheres on a silicon substrate are presented. The numerical results show that the nonzero Mueller matrix elements for scattering from a surface consisting of a monolayer of dielectric spheres on a silicon substrate have specific maxima at some scattering angles. These maxima may be used in the characterization of features of the surface. For light transmitted through the monolayer of spheres, our results show that the transmitted energy focuses around the ray passing through centers of the spheres. At other locations, the transmitted flux is very small. Therefore, micrometer-sized dielectric spheres might be placed on a semiconductor surface to burn nanometer-sized holes in a layer using laser pulses. The method may also be useful in the assembly of periodic microstructures on surfaces. © 2007 Optical Society of America

OCIS codes: 220.4000, 240.5770, 290.5880.

1. Introduction

Understanding electromagnetic scattering from surfaces is essential in the interpretation of radar observations of solid bodies, radio wave surface sounding, and many terrestrial or extraterrestrial remote-sensing problems.[1] The scattering of electromagnetic waves from, and their transmission through, random rough surfaces or surfaces with periodic roughness structures has also been of considerable interest in applications such as detection of surface defects or contamination,[2] characterization of nanometer-sized particles in crystalline structures,[3] and telecommunications.[4] The most frequently used algorithms on wave scattering from rough surfaces can be divided into two categories. The first category is to make analytical approximations, such as the small perturbation model (SPM),[5–8] the Kirchhoff approximation (KA),[9–11] the integral equation method (IEM),[12–15] and other methods.[16] The second category is based on sparse-matrix grid numerical solutions such as the finite-element method (FEM)[17,18] and the finite-difference time-domain (FDTD) technique.[19–21] The approximate approaches for light scattering and transmission by rough surfaces have limitations in their applicability. For example, the computed scattered field of the SPM is valid only for the contribution from surfaces with roughness scales much smaller than the incident wavelength; whereas, the KA is valid only when the surface roughness level is much greater than the wavelength. When the surface roughness level is similar to the wavelength such as sea-surface capillary waves under millimeter wave radar or a micrometer-sized particle layer in visible laser illumination, neither the SPM nor the KA can be applied to calculate the scattering or transmission of the light by the surface. Although the IEM model was developed to bridge the gap between the SPM and the KA models, as an approximate method, which is essentially a second iteration of the iterative KA, its accuracy still needs to be improved.[22–25] Therefore, when the surface roughness scale is sim-

W. Sun (w.sun@larc.nasa.gov) is with the Center for Atmospheric Sciences, Hampton University, Hampton, Virginia 23668 and is also with the NASA Langley Research Center, Mail Stop 420, Hampton, Virginia 23681-0001. G. Videen is with the U.S. Army Research Laboratory, Adelphi, Maryland 20783. B. Lin and Y. Hu are with the NASA Langley Research Center, Hampton, Virginia 23681.

Received 5 July 2006; revised 19 October 2006; accepted 19 October 2006; posted 20 October 2006 (Doc. ID 72736); published 12 February 2007.

0003-6935/07/071150-07$15.00/0

© 2007 Optical Society of America

ilar to the wavelength, accurate approaches based on numerical solutions of Maxwell's equations such as the FDTD technique are usually used.[26–31]

Optical probes for microelectronics manufacturing are gaining increasing importance.[32] Many applications require the characterization of materials and devices such as arrays of nanometer- or micrometer-sized particles to make crystalline structures for optical matter. For example, polystyrene spheres placed on a substrate become oriented when they are under electromagnetic illumination.[33] These spheres also tend to be attracted to regions of field maxima. The macrocrystalline structures that are formed depend on the parameters of the system: wavelength, polarization state, sphere size, etc. There is growing interest in this kind of optical matter in material sciences and thus increasing effort in measuring or modeling the optical properties of these structures. One of the downsides of modeling such structures analytically using modifications of Mie theory and the Foldy–Lax multiple-scattering equations is their complexity for multiple-particle systems and incorporating interactions with the plane surface.[34,35] In a numerical algorithm such as the FDTD, these problems are negligible and, since the system is discretized, there is little restriction on the shapes or heterogeneities of the scattering system. Although the FDTD requires significant computational time and memory, the spatial-cell-size-related numerical errors of the FDTD are negligible for most of the applications. In this study, the FDTD method is applied to calculate the scattered and transmitted electromagnetic fields of a monolayer of dielectric spheres on a silicon substrate. In Section 2, the numerical approach to calculate light-scattering and transmission properties of a surface is presented. In Section 3, features of light scattered from and transmitted through a monolayer of dielectric spheres on a silicon substrate are reported. Summary and conclusions are given in Section 4.

2. Method

The FDTD technique with periodic boundary conditions[26] and uniaxial perfectly matched layer (UPML) absorbing boundary conditions (ABC)[36,37] is used to calculate the near-electromagnetic fields scattered and transmitted by a material interface in the time domain. The time series at each grid point where near-to-far-field transformation will be done is transformed into the fields in the frequency domain using the discrete Fourier transform (DFT). The scattering and absorption quantities are calculated using the fields in the frequency domain.

Figure 1 illustrates a case of light scattering by a rough surface: Micrometer-scale particles resting on a flat silicon substrate are illuminated by visible light. Also shown in this figure are coordinate systems used in the derivation of the light-scattering formulas. We assume the surface $z = f(x, y)$ stretches infinitely in the x and y directions. The roughness features (z) of the surface are periodic in both x and y directions. The physical modeling for the FDTD algorithm is illustrated in Fig. 2. We assume the incident electromagnetic waves propagate along the z direction. In the incident direction, the computational domain is truncated by the UPML ABC.[36,37] At the sides $i = i_a$ and i_b and $j = j_a$ and j_b, periodic boundary conditions can be applied, e.g., for the x components of magnetic and electric fields:

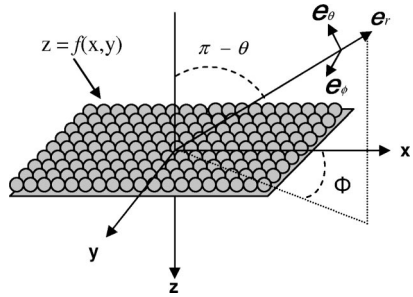

Fig. 1. Surface consisting of a monolayer of dielectric spheres on a silicon substrate and the coordinate systems used in this study. Normal radiation incidence is treated, i.e., along the z direction.

$$H_x^{n+1/2}\left(i_b, j+\tfrac{1}{2}, k+\tfrac{1}{2}\right) \leftarrow H_x^{n+1/2}\left(i_a, j+\tfrac{1}{2}, k+\tfrac{1}{2}\right), \tag{1a}$$

$$H_x^{n+1/2}\left(i, j_b+\tfrac{1}{2}, k+\tfrac{1}{2}\right) \leftarrow H_x^{n+1/2}\left(i, j_a+\tfrac{1}{2}, k+\tfrac{1}{2}\right), \tag{1b}$$

$$E_x^{n+1}\left(i_a+\tfrac{1}{2}, j, k\right) \leftarrow E_x^{n+1}\left(i_b+\tfrac{1}{2}, j, k\right), \tag{1c}$$

$$E_x^{n+1}\left(i+\tfrac{1}{2}, j_a, k\right) \leftarrow E_x^{n+1}\left(i+\tfrac{1}{2}, j_b, k\right), \tag{1d}$$

where E_x and H_x are electric and magnetic field components, respectively; $n + \frac{1}{2}$ and $n + 1$ are temporal points when the field components are updated; $\left(i, j + \frac{1}{2}, k + \frac{1}{2}\right)$ and $\left(i + \frac{1}{2}, j, k\right)$ are the magnetic and electric field-component positions in the FDTD grid, respectively. Note that magnetic and electric field components are evaluated at temporal points with half-time-step difference and spatial points with half-cell-size difference in each direction. The arrow "←" denotes the assignment of the value of the field com-

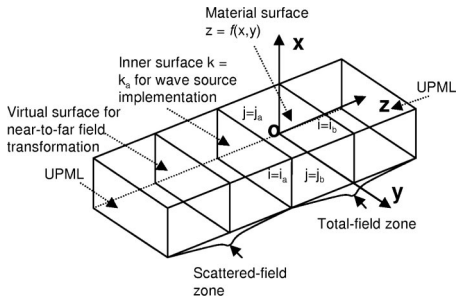

Fig. 2. Real and virtual surfaces associated with a unit periodicity. Used for implementing the FDTD algorithm for calculation of the scattered and transmitted fields near a periodic rough surface. We use periodic boundary conditions and UPML absorbing boundary conditions to truncate the computational domain.

ponent at its right side to the field component at its left side.

In this study we use the total- and scattered-field formulation[38,39] to excite the magnetic and electric fields to simulate a linearly polarized plane wave propagating to the target surface. In this formulation, the electric field is excited on an inner surface $k = k_a$ between the material surface and the UPML as shown in Fig. 2. The magnetic field is excited at $k = k_a - \frac{1}{2}$. Due to the periodic boundary conditions at sides $i = i_a$ and i_b and $j = j_a$ and j_b and because the magnetic wave is excited a half-cell size behind the electric wave, the excited electromagnetic waves can only propagate in the positive z direction. For simplicity, in this study only normal incidence is considered. Therefore, the whole computational domain is divided by the inner surface into two zones: the scattered-field zone and the total-field zone as shown in Fig. 2.

For calculation of light-scattering properties of the surface, we follow the convention in Bohren and Huffman[40] for the relation between incident and scattered Stokes parameters and the Mueller matrix as

$$\begin{bmatrix} I_s \\ Q_s \\ U_s \\ V_s \end{bmatrix} = \frac{1}{k^2R^2}\begin{bmatrix} S_{11} & S_{12} & S_{13} & S_{14} \\ S_{21} & S_{22} & S_{23} & S_{24} \\ S_{31} & S_{32} & S_{33} & S_{34} \\ S_{41} & S_{42} & S_{43} & S_{44} \end{bmatrix}\begin{bmatrix} I_0 \\ Q_0 \\ U_0 \\ V_0 \end{bmatrix}, \tag{2}$$

where k is the wavenumber and $R = |\mathbf{R}|$ where $\mathbf{R}$ denotes the position vector of the observation point. The Mueller matrix contains all the information in light scattered from a rough surface. For a full formulation of the scattering properties of a surface, the Mueller matrix is derived from the fields calculated by the FDTD method on a virtual surface in the scattered-field zone as shown in Fig. 2. For an infinite surface scattering problem, this virtual surface also must be infinite. However, the near- to far-field transformation by an integral of the fields on an infinite surface is computationally impractical. In this study we derive the Mueller matrix using the magnetic and electric fields in the frequency domain on the virtual surface corresponding to the period of the material surface.

On the virtual surface, the tangential components of the scattered near fields in the frequency domains $\mathbf{E}^s$ and $\mathbf{H}^s$ are calculated first using the FDTD method. The scattered far fields can be computed in terms of the equivalent surface electric current $\mathbf{J}$ and magnetic current $\mathbf{M}$ on the virtual surface. The equivalent surface currents are computed by

$$\mathbf{J} = \mathbf{n} \times \mathbf{H}^s, \tag{3a}$$

$$\mathbf{M} = -\mathbf{n} \times \mathbf{E}^s, \tag{3b}$$

where $\mathbf{n}$ is the outward unit normal vector on the virtual surface. In spherical coordinates as shown in Fig. 1, the scattered electric far-field components for the θ and ϕ polarizations are given as follows[21]:

$$E_\theta \approx -\frac{ik\exp(-ikR)}{4\pi R}(L_\phi + \eta_0 N_\theta), \tag{4a}$$

$$E_\phi \approx +\frac{ik\exp(-ikR)}{4\pi R}(L_\theta - \eta_0 N_\phi), \tag{4b}$$

where $\eta_0 = \sqrt{\mu_0/\varepsilon_0}$ is the intrinsic impedance of free space and L_θ, L_ϕ and N_θ, N_ϕ are the θ and ϕ components of the following vectors:

$$\mathbf{L} = \iint_s (\mathbf{x}M_x + \mathbf{y}M_y + \mathbf{z}M_z)\exp(ik\mathbf{r}'\mathbf{r})\mathrm{d}s', \tag{5a}$$

$$\mathbf{N} = \iint_s (\mathbf{x}J_x + \mathbf{y}J_y + \mathbf{z}J_z)\exp(ik\mathbf{r}'\mathbf{r})\mathrm{d}s', \tag{5b}$$

where $\mathbf{x}$, $\mathbf{y}$, and $\mathbf{z}$ denote the unit vectors in the x, y, and z directions, respectively, $\mathbf{r}$ denotes the unit vector in the scattering direction, $\mathbf{r}'$ is the vector for the current's position on the virtual surface s, M_x, M_y, M_z and J_x, J_y, J_z are the components of magnetic current $\mathbf{M}$ and electric current $\mathbf{J}$, respectively. For reasonable accuracy in calculations of the scattering properties from an infinite surface, the integral area s in Eqs. (5a) and (5b) must be many periods of the virtual surface (see Section 3). Although the FDTD computes only the magnetic and electric fields on one period of the virtual surface, the fields on a single period of the virtual surface can be used repeatedly in Eqs. (5a) and (5b) for other periods of virtual surface s. However, when many periods are involved in the calculation, Eqs. (5a) and (5b) in their original forms are very time consuming. Due to the periodic nature of the studied surface and the scattered light, Eqs. 5(a) and 5(b) can be simplified to the following computationally efficient forms:

$$\mathbf{L} = \delta\iint_{s_0} (\mathbf{x}M_x + \mathbf{y}M_y + \mathbf{z}M_z)\exp(ik\mathbf{r}'\mathbf{r})\mathrm{d}s', \tag{6a}$$

$$\mathbf{N} = \delta\iint_{s_0} (\mathbf{x}J_x + \mathbf{y}J_y + \mathbf{z}J_z)\exp(ik\mathbf{r}'\mathbf{r})\mathrm{d}s', \tag{6b}$$

where s_0 denotes the area of a single period of virtual surface s, and δ is a factor accounting for the contributions from all periods of the infinite surface in the form:

$$\delta = \sum_{m=-\infty}^{\infty}\sum_{n=-\infty}^{\infty} \exp[ik\mathbf{r}\cdot(mp_x,\ mp_y,\ 0)], \tag{7}$$

where p_x and p_y are the period lengths in the x and y directions, respectively. Related to scattering inten-

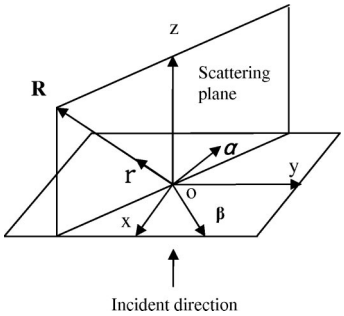

Fig. 3. Coordinate systems for the derivation of scattering matrix elements. The unit vectors $\boldsymbol{\alpha}$, $\boldsymbol{\beta}$, and $\mathbf{r}$ are orthogonal. $\mathbf{r}$ is in the scattering direction, and $\boldsymbol{\beta}$ is perpendicular to the scattering plane.

sity, δ is a two-dimensional delta function of scattering angle, which gives infinitely large values in the backscattering direction. In practice, the summation of Eq. (7) cannot be done for infinite m and n. The cutoff for m and n causes errors in δ values and results in errors in the calculated Mueller matrix elements.

The Mueller matrix is derived from the amplitude scattering matrix elements. To calculate the amplitude scattering matrix elements, the scattered field is decomposed into the components parallel and perpendicular to the scattering plane as shown in Fig. 3.[41,42] So we have

$$\mathbf{E}(\mathbf{R}) = \boldsymbol{\alpha} E_{\alpha}(\mathbf{R}) + \boldsymbol{\beta} E_{\beta}(\mathbf{R}), \tag{8}$$

where $\boldsymbol{\alpha}$ and $\boldsymbol{\beta}$ denote the unit vectors parallel and perpendicular to the scattering plane as shown in Fig. 3, respectively, and $\boldsymbol{\beta} \times \boldsymbol{\alpha} = \mathbf{r}$.

Based on the definition of the amplitude scattering matrix, we have the transformation equation for light scattered by the surface as

$$\begin{bmatrix} E_{\alpha}(\mathbf{R}) \\ E_{\beta}(\mathbf{R}) \end{bmatrix} = \frac{\exp(-ikR)}{ikR} \begin{bmatrix} s_2 & s_3 \\ s_4 & s_1 \end{bmatrix} \begin{pmatrix} E_{0,\alpha} \\ E_{0,\beta} \end{pmatrix}, \tag{9}$$

where $E_{0,\alpha}$ and $E_{0,\beta}$ are the parallel and perpendicular incident field components with respect to the scattering plane. $E_{0,\alpha}$ and $E_{0,\beta}$ are related to the x- and y-polarized incident fields used in the FDTD simulation with

$$\begin{pmatrix} E_{0,\alpha} \\ E_{0,\beta} \end{pmatrix} = \begin{bmatrix} \boldsymbol{\beta}\cdot\mathbf{x} & -\boldsymbol{\beta}\cdot\mathbf{y} \\ \boldsymbol{\beta}\cdot\mathbf{y} & \boldsymbol{\beta}\cdot\mathbf{x} \end{bmatrix} \begin{pmatrix} E_{0,y} \\ E_{0,x} \end{pmatrix}. \tag{10}$$

Therefore, using Eqs. (4a), (4b), (9), and (10), along with $E_{\theta} = E_{\alpha}$ and $E_{\phi} = -E_{\beta}$, we have the amplitude scattering matrix

$$\begin{bmatrix} s_2 & s_3 \\ s_4 & s_1 \end{bmatrix} = \begin{bmatrix} F_{\alpha,y} & F_{\alpha,x} \\ F_{\beta,y} & F_{\beta,x} \end{bmatrix} \begin{bmatrix} \boldsymbol{\beta}\cdot\mathbf{x} & \boldsymbol{\beta}\cdot\mathbf{y} \\ -\boldsymbol{\beta}\cdot\mathbf{y} & \boldsymbol{\beta}\cdot\mathbf{x} \end{bmatrix}, \tag{11}$$

where the quantities $F_{\alpha,x}$, $F_{\beta,x}$, and $F_{\alpha,y}$, $F_{\beta,y}$ are calculated for x- and y-polarized incident light, respectively, in forms:

(1) For x-polarized incidence,

$$\begin{pmatrix} F_{\alpha,x} \\ F_{\beta,x} \end{pmatrix} = \frac{k^2}{4\pi} \begin{pmatrix} L_{\phi} + \eta_0 N_{\theta} \\ L_{\theta} - \eta_0 N_{\phi} \end{pmatrix}; \tag{12}$$

(2) For y-polarized incidence,

$$\begin{pmatrix} F_{\alpha,y} \\ F_{\beta,y} \end{pmatrix} = \frac{k^2}{4\pi} \begin{pmatrix} L_{\phi} + \eta_0 N_{\theta} \\ L_{\theta} - \eta_0 N_{\phi} \end{pmatrix}. \tag{13}$$

From these elements, all the elements of the Mueller matrix can be calculated. Since the calculation accuracy of the Mueller matrix is also a function of the virtual surface area s, when s is infinitely large, the Mueller matrix approaches exact. To approximate the infinite-surface Mueller matrix with a limited number of surface periods, we rewrite the relation between incident and scattered Stokes parameters in a new form:

$$\begin{bmatrix} I_s/s \\ Q_s/s \\ U_s/s \\ V_s/s \end{bmatrix} = \frac{S_{11}/(k^2 s)}{R^2} \begin{bmatrix} 1 & S_{12}/S_{11} & S_{13}/S_{11} & S_{14}/S_{11} \\ S_{21}/S_{11} & S_{22}/S_{11} & S_{23}/S_{11} & S_{24}/S_{11} \\ S_{31}/S_{11} & S_{32}/S_{11} & S_{33}/S_{11} & S_{34}/S_{11} \\ S_{41}/S_{11} & S_{42}/S_{11} & S_{43}/S_{11} & S_{44}/S_{11} \end{bmatrix} \times \begin{bmatrix} I_0 \\ Q_0 \\ U_0 \\ V_0 \end{bmatrix}, \tag{14}$$

where I_s/s, Q_s/s, U_s/s, and V_s/s denote the scattered Stokes parameters per unit area of the surface. In Eq. (14), $S_{11}/(k^2 s)$ is a normalized phase function, which accounts for the reflectance at each scattering angle. Therefore the integration of $S_{11}/(k^2 s)$ over the half-space above the scattering surface equals the scattering efficiency (albedo), i.e.,

$$\int_0^{2\pi} \int_{\pi/2}^{\pi} \left[S_{11}/(k^2 s)\right] \sin\theta \mathrm{d}\theta \mathrm{d}\phi = Q_{sca}. \tag{15}$$

The normalized phase function requires an integral over large s to approach its exact correspondence because of the errors in obtaining the δ factor from a limited number of surface periods. However, since the $|\delta|^2$ factor exists in all the Mueller matrix elements, the ratios of the Mueller matrix elements to S_{11} are not affected by the δ factor and their accuracies are determined simply by the FDTD calculation for a single period of the surface.

3. Numerical Results

Bidirectional reflectance distribution function (BRDF) and bidirectional transmittance distribution function (BTDF) are usually measured to characterize crystalline structures. Numerical calculation of the BRDF or BTDF of crystalline structures can directly link their optical characteristics with their geometric and physical properties. Therefore, numerical simulation of the

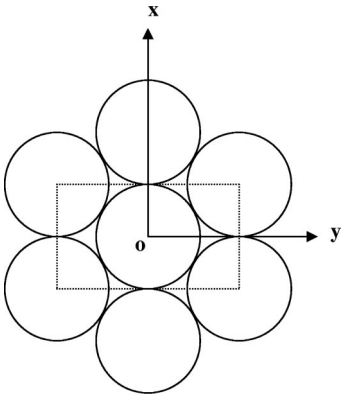

Fig. 4. Geometry of one period in the surface of a monolayer of dielectric spheres on a silicon substrate.

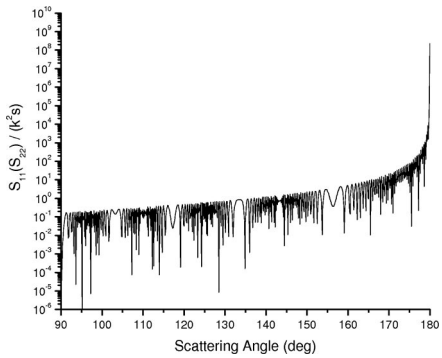

Fig. 5. Normalized light-scattering phase function $S_{11}/(k^2s)$ computed with the FDTD scheme for a flat silicon substrate of refractive index $m = 4.90 + 3.84i$ at a normal incidence of $\lambda_0 = 308$ nm. Calculations are performed using a 308 nm × 308 nm substrate period and integrations over 2001 × 2001 periods. Since normal incidence is used, this curve should be a delta function in the backscattering direction (180° of phase angle). The curve therefore shows the magnitude and character of the computational noise.

BRDF or BTDF of material interfaces could be the basis for accurate characterization of crystalline structures. In this section, we present the computational results related to the BRDF and BTDF for light scattered from and transmitted through a monolayer of micrometer-sized dielectric spheres on a silicon substrate as shown in Fig. 1. As discussed later, this kind of particle-substrate structure might be used in burning nanometer-sized hole arrays in a layer under laser radiation, which may have various applications in nanotechnology. In this study, the spheres on the substrate are touching and in a hexagonal configuration. Although the simplest base for this crystalline structure is hexagonal, as shown in Fig. 4, we can use a periodic rectangular grid with a sphere in the center and the rectangular box passing through the centers of the adjacent spheres for the FDTD calculation to simulate the light scattering and transmission by the surface structure. In this simulation, the incident wavelength is $\lambda_0 = 308$ nm, and the refractive indices of the spheres and the silicon substrate are $m = 1.64$ and $m = 4.90 + 3.84i$, respectively. The radii of the spheres are 510 nm. We are interested in both the near fields transmitted in the silicon substrate and the far fields scattered by the sphere-substrate surface in free space. In the FDTD calculations, we use a six-cell UPML to truncate the free space and a six-cell UPML on the other end to truncate the material space. The cubic spatial cell size for the FDTD is set to be $\Delta s = \lambda_0/60$. For comparison with the light-scattering features of the surface of the silicon substrate and the micrometer-sized spheres, the normalized phase function and the Mueller matrix elements of the simple flat substrate are also calculated.

Figure 5 shows the azimuthally averaged normalized light-scattering phase function of the flat silicon substrate under normal incidence. For this flat-surface scattering calculation, the FDTD simulation is run on a 308 nm × 308 nm substrate period. The transformation of near to far field is done with an integration of the near fields over 2001 × 2001 periods of the surface. We can see that most of the scattered energy concentrates in a very small solid angle around the backscattering direction (i.e., at a scattering angle of 180°). However, due to the limited number of periods of surface area that are used to approximate the normalized phase function, a small amount of scattered energy can still be found at other scattering angles, although that intensity is several orders lower than the backscattered peak. For light scattering by the surface of the monolayer of spheres and the silicon substrate (Fig. 6), the azimuthally averaged normalized light-scattering phase function has two specific maxima (numbered 2 and 3) at the scattering angles of ~115° and ~145°, respectively. These maxima are side scattering by the spheres on the substrate and may be used in the characterization of features of the surface. However, for characterization of this kind of surface, the polarization features of scattered light might contain the most useful information. Figures 7(a)–7(c) show the nonzero azimuthally averaged normalized Mueller matrix elements of the monolayer of spheres and the silicon substrate. Also shown in these figures are the results for light scattered simply by the flat substrate. We can see that the polarization degree of the

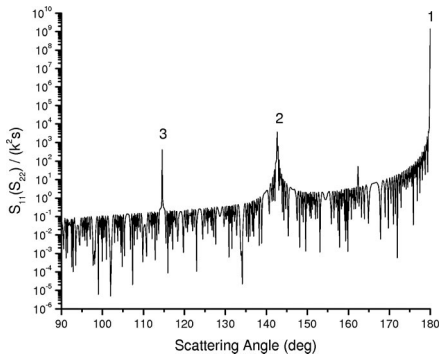

Fig. 6. Normalized light-scattering phase function $S_{11}/(k^2s)$ computed with the FDTD scheme for a monolayer of spheres with a radius of 510 nm and a refractive index of 1.64 on the silicon substrate of Fig. 5. Peaks with high signal-to-noise ratios emerge.

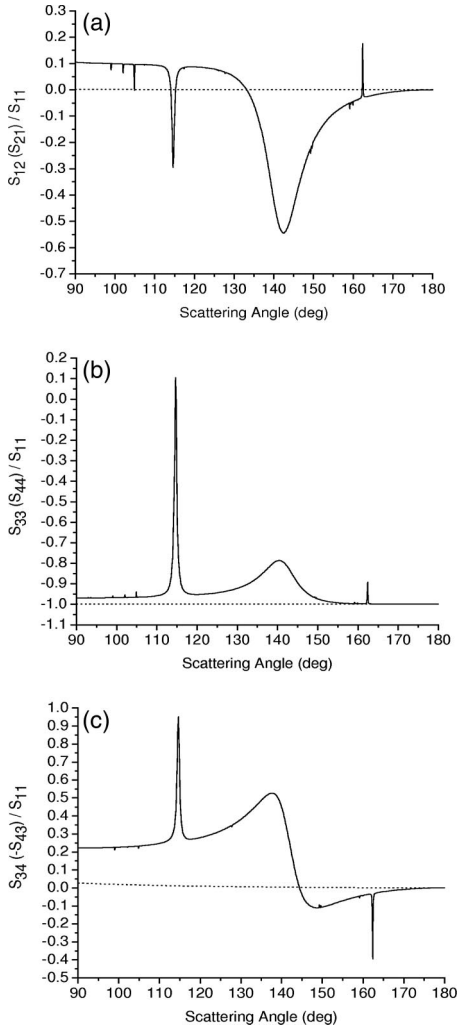

Fig. 7. Normalized Muller matrix elements computed with the FDTD scheme for a monolayer of dielectric spheres with a radius of 510 nm and a refractive index of 1.64 on a silicon substrate under normal incidence: (a) $S_{12}(S_{21})/S_{11}$, (b) $S_{33}(S_{44})/S_{11}$, and (c) $S_{34}(-S_{43})/S_{11}$. Also shown are the corresponding normalized Muller matrix elements of the noise, i.e., of computations for the flat silicon substrate, in dashed curves. These polarization quantities give more information about the surface than the total scattering.

scattered light from simply the flat substrate and that from the substrate with the spherical particles are significantly different. At the scattering angle of $\sim 115°$, $S_{12}(S_{21})/S_{11}$, $S_{33}(S_{44})/S_{11}$, and $S_{34}(-S_{43})/S_{11}$ all show a strong peak corresponding to maximum 3 as shown in Fig. 6. Because these quantities are independent of the number of periods in the near- to far-field transformation integration, their accuracies in the numerical calculation are high and solely determined by the FDTD technique. Furthermore, corresponding to maximum 2 in Fig. 6, $S_{12}(S_{21})/S_{11}$, $S_{33}(S_{44})/S_{11}$, and $S_{34}(-S_{43})/S_{11}$ all have maxima, especially in the linear polarization degree $S_{12}(S_{21})/S_{11}$. This polarization feature of scattered light can be detected easily using polarimetry. For light transmitted through the monolayer of spheres, we calculate the energy flux $\lambda_0/30$ deep inside the substrate for a

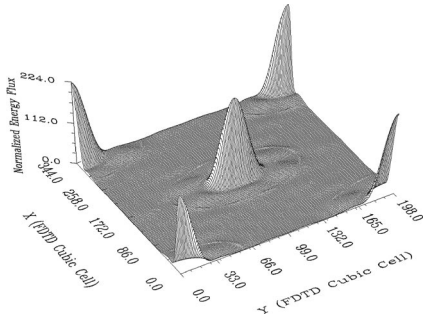

Fig. 8. Normalized transmitted light flux at a depth of $\lambda_0/30$ inside the silicon substrate for a period of the rough surface, as shown in Fig. 4. The unit for both x and y axes in this figure is the FDTD cubic cell size, i.e., $\Delta s = \lambda_0/60$. Micrometer-sized dielectric spheres might be placed on a semiconductor surface to burn nanometer-sized holes in a layer using laser pulses.

period of the surface system. Figure 8 shows the spatial distribution of the transmitted flux normalized by the incident flux. We can see that the transmitted energy focuses around the ray passing through centers of the spheres. At other locations, the transmitted flux is very small. Therefore, transmitted laser light distributed by the micrometer-sized sphere structures can make nanometer-sized structures on the substrate, which have been observed by atomic force microscopy.

4. Summary and Conclusions

Light scattering and transmission by rough surfaces are of considerable interest in a variety of applications including remote sensing, characterization of surfaces, and making nanometer-sized structures. In this study, the finite-difference time domain technique is applied to calculate the scattered and transmitted electromagnetic fields near a period of an infinite periodic rough surface. The elements of the Mueller matrix for scattered light are calculated by an integral of the near fields over a significant number of periods of the surface. The normalized Mueller matrix elements of the scattered light and the field density of transmitted light for a monolayer of dielectric spheres on a silicon substrate are calculated. The numerical results show that the nonzero Mueller matrix elements of the system of a monolayer of dielectric spheres on a silicon substrate have two specific maxima at the scattering angles of $\sim 115°$ and $\sim 145°$, respectively. These maxima may be used in the characterization of the system for quality control in making these kinds of structure. For light transmitted through the monolayer of spheres, our results show that the transmitted energy focuses around the ray passing through centers of the spheres. At other locations, the transmitted flux is very small. Therefore, micrometer-sized dielectric spheres might be placed on a semiconductor surface to burn nanometer-sized holes in a layer using laser pulses.

The authors thank Erhard Rothe of Wayne State University for helpful communications on the sphere-substrate structures.

References

1. D. L. Schuler, J.-S. Lee, D. Kasilingam, and G. Nesti, "Surface roughness and slope measurements using polarimetric SAR data," IEEE Trans. Geosci. Remote Sens. **40,** 687–698 (2002).
2. S. Gomez, K. Hale, J. Burrows, and B. Griffiths, "Measurements of surface defects on optical components," Meas. Sci. Technol. **9,** 607–616 (1998).
3. H. Lin and J. Zhu, "Characterization of nanocrystalline silicon films," Proc. SPIE **4700,** 354–356 (2002).
4. H. Budiarto and J. Takada, *The Electromagnetic Wave Scattering from Building Surfaces for the Mobile Propagation Modeling,* ITE Technical Report 25 (ITE, 2001), pp. 7–11.
5. Lord Rayleigh, *The Theory of Sound* (MacMillan, 1896).
6. U. Fano, "The theory of anomalous diffraction gratings and of quasi-stationary waves on metallic surfaces (Sommerfeld's waves)," J. Opt. Soc. Am. **31,** 213–222 (1941).
7. S. O. Rice, "Reflection of electromagnetic waves from slightly rough surfaces," Commun. Pure Appl. Math. **4,** 351–378 (1951).
8. S. O. Rice, *Reflection of EM from Slightly Rough Surfaces* (Interscience, 1963).
9. C. Eckart, "The scattering of sound from the sea surface," J. Acoust. Soc. Am. **25,** 66–570 (1953).
10. H. Davies, "The reflection of electromagnetical waves from rough surfaces," Proc. Inst. Electr. Eng. **101,** 209–214 (1954).
11. P. Beckmann and A. Spizzichino, *Scattering of Electromagnetic Waves from Rough Surfaces* (Pergamon, 1963).
12. A. K. Fung and G. W. Pan, "An integral equation method for rough surface scattering," in *Proceedings of the International Symposium on Multiple Scattering of Waves in Random Media and Random Surfaces* (1986), pp. 701–714.
13. A. K. Fung, Z. Li, and K. S. Chen, "Backscattering from a randomly rough dielectric surface," IEEE Trans. Geosci. Remote Sens. **30,** 356–369 (1992).
14. A. K. Fung, *Microwave Scattering and Emission Models and Their Applications* (Artech House, 1994).
15. L. Tsang, J. A. Kong, K. H. Ding, and C. O. Ao, *Scattering of Electromagnetic Waves: Numerical Simulations* (Wiley, 2001).
16. M. Saillard and A. Sentenac, "Rigorous solutions for electromagnetic scattering from rough surfaces," Waves Random Media **11,** 103–137 (2001).
17. P. P. Silvester and R. L. Ferrari, *Finite Elements for Electrical Engineers* (Cambridge U. Press, 1990).
18. J. M. Jin, *The Finite Element Method in Electromagnetics* (Wiley, 1993).
19. K. S. Yee, "Numerical solution of initial boundary value problems involving Maxwell's equations in isotropic media," IEEE Trans. Antennas Propag. **AP-14,** 302–307 (1966).
20. K. S. Kunz and R. J. Luebbers, *The Finite Difference Time Domain Method for Electromagnetics* (CRC Press, 1993).
21. A. Taflove, *Computational Electrodynamics: The Finite-Difference Time-Domain Method* (Artech House, 1995).
22. C. Y. Hsieh, A. K. Fung, G. Nesti, A. J. Siber, and P. Coppo, "A further study of the IEM surface scattering model," IEEE Trans. Geosci. Remote Sens. **35,** 901–909 (1997).
23. A. K. Fung, Z. Li, and K. S. Chen, "An improved IEM model for bistatic scattering from rough surfaces," J. Electromagn. Waves Appl. **16,** 689–702 (2002).
24. K. S. Chen, T. D. Wu, and A. K. Fung, "A study of backscattering from multiscale rough surface," J. Electromagn. Waves Appl. **12,** 961–979 (1998).
25. F. Mattia, "Backscattering properties of multi-scale rough surfaces," J. Electromagn. Waves Appl. **13,** 493–527 (1999).
26. C. H. Chan, S. H. Lou, L. Tsang, and J. A. Kong, "Electromagnetic scattering of waves by rough surfaces: a finite-difference time-domain approach," Microwave Opt. Technol. Lett. **4,** 355–359 (1991).
27. A. K. Fung, M. R. Shah, and S. Tjuatja, "Numerical simulation of scattering from three-dimensional randomly rough surfaces," IEEE Trans. Geosci. Remote Sens. **32,** 986–994 (1994).
28. F. D. Hastings, J. B. Schneider, and S. L. Broschat, "A Monte-Carlo FDTD technique for rough surface scattering," IEEE Trans. Antennas Propag. **43,** 1183–1191 (1995).
29. R. J. Luebbers and C. Penney, "Scattering from apertures in infinite ground planes using FDTD," IEEE Trans. Antennas Propag. **42,** 731–736 (1994).
30. K. Demarest, R. Plumb, and Z. Huang, "FDTD modeling of scatterers in stratified media," IEEE Trans. Antennas Propag. **43,** 1164–1168 (1995).
31. P. B. Wong, G. L. Tyler, J. E. Baron, E. M. Gurrola, and R. A. Simpson, "A three-wave FDTD approach to surface scattering with applications to remote sensing of geophysical surfaces," IEEE Trans. Antennas Propag. **44,** 504–513 (1996).
32. F. Moreno, F. Gonzalez, J. M. Saiz, P. J. Valle, and D. L. Jordan, "Experimental study of copolarized light scattering by spherical metallic particles on conducting flat substrates," J. Opt. Soc. Am. A **10,** 141–149 (1993).
33. J. Mullins, "The stuff of beams," New Sci. **190,** 44–47 (2006).
34. T. M. Grzegorczyk, B. A. Kemp, and J. A. Kong, "Trapping and binding of an arbitrary number of cylindrical particles in an in-plane electromagnetic field," J. Opt. Soc. Am. A **23,** 2324–2330 (2006).
35. T. M. Grzegorczyk, B. A. Kemp, and J. A. Kong, "Stable optical trapping based on optical binding forces," Phys. Rev. Lett. **96,** 113903 (2006).
36. Z. S. Sacks, D. M. Kingsland, R. Lee, and J.-F. Lee, "A perfectly matched anisotropic absorber for use as an absorbing boundary condition," IEEE Trans. Antennas Propag. **43,** 1460–1463 (1995).
37. S. D. Gedney, "An anisotropic perfectly matched layer-absorbing medium for the truncation of FDTD lattices," IEEE Trans. Antennas Propag. **44,** 1630–1639 (1996).
38. D. E. Merewether, R. Fisher, and F. W. Smith, "On implementing a numeric Huygen's source in a finite difference program to illustrate scattering bodies," IEEE Trans. Nucl. Sci. **NS-27,** 1829–1833 (1980).
39. K. Umashanker and A. Taflove, "A novel method to analyze electromagnetic scattering of complex objects," IEEE Trans. Electromagn. Compat. **EMC-24,** 397–405 (1982).
40. C. F. Bohren and D. R. Huffman, *Absorption and Scattering of Light by Small Particles* (Wiley, 1983).
41. P. Yang and K. N. Liou, "Finite-difference time domain method for light scattering by small ice crystals in three-dimensional space," J. Opt. Soc. Am. A **13,** 2072–2085 (1996).
42. W. Sun, N. G. Loeb, and Q. Fu, "Finite-difference time domain solution of light scattering and absorption by particles in an absorbing medium," Appl. Opt. **41,** 5728–5743 (2002).